Fine structure of Rydberg states. III. New measurements in D, F, and G states of ^{4}He†

Keith B. MacAdam
Department of Physics, University of Arizona, Tucson, Arizona 85721

William H. Wing
Department of Physics and Optical Sciences Center, University of Arizona, Tucson, Arizona 85721

(Received 16 August 1976)

We report further accurate measurements of fine structure in D, F, and G Rydberg states of ^{4}He obtained using a microwave-optical resonance method and electron-bombardment excitation. Single-quantum electric-dipole transitions $10\,^1D_2$-$10\,^{1,3}F_3$, $11\,^1D_2$-$11\,^{1,3}F_3$, $12\,^3D_J$-$12\,^{1,3}F_{J'}$, and $6\,^1F_3$-$6\,^1G_4$ and two-quantum transitions $7\,^1D_2$-$7\,^{1,3}G_4$, $9\,^1D_2$-$9\,^{1,3}G_4$, $10\,^3D_J$-$10\,^{1,3}G_{J'}$, and $16\,^1P$-$16\,^{1,3}F_3$ were observed. Both electrostatic and relativistic fine-structure intervals were determined with uncertainties less than 1 MHz and are compared with theoretical results. The data constitute the first measurements of G-state fine structure in helium. Series formulas incorporating all our measurements are given for serveral resonance series, and we show that the entire series $n\,^1F_3$-$n\,^1G_4$ can be predicted to within 75 ppm.

I. INTRODUCTION

Our measurements of electrostatic and relativistic fine structure (fs) in highly excited (Rydberg) states of ^{4}He have been described in several publications.[1-6] The two recent detailed reports, Ref. 5 (referred to hereafter as I) and Ref. 6 (II), have discussed the microwave-optical method[7,8] and apparatus used and have given results for D-F transitions in principal quantum numbers $n = 6$–9 and P-D transitions in $n = 16$–18. This paper reports further measurements using an improved apparatus and both one- and two-quantum rf transitions as follows: D-F transitions in $n = 10$–12; an F-G transition in $n = 6$; D-G transitions in $n = 7$, 9, and 10; and ^1P-F transitions in $n = 16$. The $16\,^1P_1$-$16\,^1D_2$ transition, reported in II, was remeasured as a test of the new apparatus. As before, the atoms were excited by electron bombardment.

Our previous work[1-6] and that of others[9-12] has stimulated theoretical calculations of helium fs by Chang and Poe.[13,14] Recent measurements of $n\,^1D$-$n\,^3D$ intervals using anticrossing methods have been made for $n = 3$–8 by Miller *et al.*[11] and by Derouard *et al.*[12] and for $n = 8$–20 by Beyer and Kollath,[15] who have also measured electrostatic fs intervals between $n\,^{1,3}D$ and G, H, I, and K states ($L = 4$–7).[16] The microwave-optical measurements have the smallest experimental uncertainties (less than 1 MHz); the anticrossing methods allow the measurement of some different but related quantities in both lower and higher n values.

A flurry of interest[17] in highly excited atomic states has resulted in several reports of Rydberg-state fs measurements in alkalis using laser excitation.[18-23] Gallagher *et al.*[19,23] obtained rf resonances by this method, and their measurements cover sodium d, f, g, and h states for $n = 11$–17. Other workers have achieved excitation of higher n states, to at least $n = 85$,[24] and higher angular momentum, to at least $l = 15$.[25]

In Sec. II, we outline the theory of the microwave-optical method for two-quantum rf transitions. The apparatus modifications are described in Sec. III. Results for single-quantum and two-quantum transitions are given in Secs. IV and V, respectively. Section VI includes discussion of series formulas for modeling Rydberg-state fs and comparisons of electrostatic and relativistic fs results with theory.

II. MICROWAVE OPTICAL METHOD USING TWO-QUANTUM TRANSITIONS

A microwave-optical method for observing resonances in short-lived excited states of atoms was described in detail by Lamb and Sanders[7] and by Wilcox and Lamb.[8] The Lamb-Sanders treatment, reviewed in I, concerned systems in which only two excited levels participate in the resonance, whereas the Wilcox-Lamb theory encompasses many levels. Both use density matrix methods to show that rate equations can be written for the excited state populations under the usual experimental conditions.

The two-quantum resonances observed in our experiments satisfied the condition $\hbar\omega_1 + \hbar\omega_2 = E_a - E_b$, where $E_a - E_b$ is the energy difference between upper and lower states, and ω_1 and ω_2 are the (possibly identical) angular frequencies of the perturbations. The oscillating perturbations were not resonant with single-quantum tran-

sitions from a or b to any other atomic states. Under these conditions, the many-level problem can be reduced to an effective two-level problem by using time-dependent perturbation theory, applying the rotating-wave approximation, and using the fact that all intermediate states in the transition are far from resonance. In the case of a single perturbation at frequency ω, the effective matrix element that couples states a and b is

$$V_{\text{eff}} = \frac{1}{2} \sum_n V_{an} V_{nb} \frac{1}{\omega - (E_n - E_b)/\hbar}. \quad (1)$$

Here we have assumed that intermediate states n lie between a and b in energy, and only the dominant terms have been retained. The perturbation is assumed to be an oscillating electric field $\vec{E}_0 \cos\omega t$, and $V_{ij} = \langle i | e\vec{E}_0 \cdot \vec{r}/\hbar | j \rangle$ is its matrix element between states i and j. The effective perturbation can be substituted into Eq. (3) of I to find the resonance lineshape. A new feature revealed by the perturbation-theory method is the rf Stark shift, a displacement of the apparent resonance center that is linear in the rf power of each oscillator. As in the exact two-level case, the resonances have Lorentzian form, exhibit saturation and power broadening, and have an irreducible width $\Delta\omega = \gamma_a + \gamma_b$ (FWHM), where γ_a and γ_b are the radiative decay rates of a and b.

The theory of multiple-quantum resonances has been worked out in considerable detail by a number of authors, whose works should be consulted for further details.[26-30]

III. APPARATUS

A. Interaction region

In the course of the work described in II, we noted distortion and line shifts due to electrostatic charging in the interior of the X-band (8.0–12.4 GHz) waveguide section (the module) where the excited atoms were produced and studied. Such effects had been unimportant until that time because the contamination of the module was a gradual process (resulting probably from pump oil migrating backward through the turbomolecular pump and the use of helium gas of inferior purity) and because no such serious demands had been made on the module as were made in the study of $n = 16$, 17, and 18 states. The X-band waveguide module described in I and II could not be baked and presented for potential contamination large surface areas that were exposed to the electron beam used for excitation of the Rydberg states and which lay near to the excited atoms themselves. Furthermore, light was collected only from small holes in the side of the waveguide, thus limiting the signal size. The fixed short at the end of the waveguide caused a standing-wave pattern whose nodal positions relative to the volume of excited atoms depended on frequency. In fact, at certain frequencies a node might be exactly coincident with the interaction region. For these reasons, we replaced the X-band module with a type not previously used in these experiments, which was intended as a prototype upon which further improvements could be based.

The new module is illustrated in Fig. 1. An unfocused electron beam is extracted from a Philips type-A dispenser cathode[31] through an accelerating grid G1 of woven tungsten mesh. The cathode K stands at a negative potential with respect to ground; this potential thus determines the kinetic energy of the electron bombardment. G1 and all other electrodes in the module are at ground potential. A second such grid G2 prevents the small fields that penetrate G1 from reaching the interaction region. The interaction region is surrounded by an array of eighteen 0.25-mm-diam tungsten wires stretched parallel to the electron beam between the peripheries of two woven-mesh grids B1 and B2 that form the ends of a cylindrical enclosure (the cage). Electrons that pass through the cage are collected by a flat plate collector C. A dc current as great as 30 A can be passed

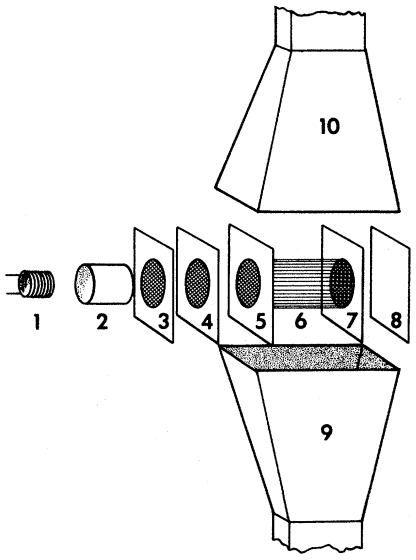

FIG. 1. Exploded view of the resonance module: (1) heater; (2) Philips cathode; (3) accelerating grid G1; (4) grid G2; (5) grid B1; (6) the "cage," consisting of wires joining the perimeters of grids B1 and B2; (7) grid B2; (8) collector C; (9) and (10) X-band waveguide horns. The grid supports are nonmagnetic stainless-steel plates, 2.54 cm square. The cage is 2.54 cm long by 1.6 cm diameter.

through the longitudinal wires of the cage from the electrodes that support B1 and B2, heating the tungsten wires to bright red heat (1300 K).

The electron-beam current is regulated by a feedback circuit that adjusts the cathode temperature to stabilize the current that reaches the collector and the electrodes of the cage. Beam currents 30–1000 μA were used in the measurements reported below.

Fluorescence of excited atoms is collected and focused by an ellipsoidal light pipe whose foci are positioned at the center of the interaction region and at the entrance slit of a $\frac{1}{4}$-m monochromator, as described in I. The geometrical transparency of the cylindrical cage is probably much greater than that of the X-band module formerly used.

Microwave radiation is incident from two X-band 10-dB rectangular waveguide horns situated directly adjacent to and on opposite sides of the cage, with the E-field polarization perpendicular to the wires of the cage. This direction of polarization minimizes the perturbing effect of the wires on the microwave transmission through the cage. Aside from the small microwave reflections set up by the wires of the cage, no standing-wave pattern should result in the interaction region since the rf energy incident from one horn is collected by the other horn and dissipated in a matched load elsewhere. The two horns also provide a convenient method for exposing the excited atoms to rf power from two separate oscillators, provided that the frequencies are above 6.6 GHz, the cut-off frequency of X-band waveguide.

The interaction region lies in the near field of each horn and is surrounded by an enclosure (the cage) whose reflective properties are very complex. We found that 50% of the power incident on the cage from one horn at 10 GHz was received in the other horn, and only 1% was reflected back into the sending horn. Aside from this, no attempt was made to calibrate the rf electric field at the interaction region in terms of the power incident in the waveguides at various frequencies. Except for the unlikely possibility that the cage could form a high-Q resonator, it should be reasonably broadband and free of standing waves. The lack of rf calibration prevents accurate estimation of the rf-power requirements or the rf Stark shifts from first principles in terms of atomic matrix elements. In the case of a two-quantum D-G transition using a single oscillator, the optimum perturbation[5] is obtained when the incident plane-wave rf power per unit area is approximately

$$S_0 = \frac{2\hbar[\omega - (E_n - E_b)/\hbar](\gamma_D \gamma_G)^{1/2}}{9\pi\alpha a_0^2 n^4}, \qquad (2)$$

where α is the fine-structure constant and a_0 is the Bohr radius. In (2) it is assumed that $n \gg l$, and a hydrogenic approximation is used. In the case of the $9\,^1D$-$9G$ transitions (Sec. V A) the optimum power density is on the order of 2×10^{-4} W/cm^2. If the rf power transmitted in the waveguide is considered to be spread uniformly into a TEM plane wave over the area of the open end of the horn, the optimum power density corresponds to approximately 2.4 mW in the waveguide. The power actually used was an order of magnitude greater than this, but the estimate is still reasonable in view of the losses between the power-measuring device and the module, the neglect of the effects of the wire cage, the neglect of singlet-triplet mixing in the G states, and the fact that resonances were measured at higher than optimum power, in order to improve the signal-to-noise ratios.

The cage was baked at red heat periodically during the experiments. We found some residual effects of charging in the module, e.g. small center shifts of the most sensitive resonances that were approximately proportional to the square of the bombarding voltage. The most likely origin of this effect is the grids B1 and B2 or their supporting electrodes, which are bombarded by the uncollimated electron beam during operation and which do not reach the red heat of the rest of the cage during bakeout. Insulating patches on the stainless-steel surfaces of the supporting electrodes that result from contamination or metallurgical effects would charge to the cathode potential, and the resulting electric fields would penetrate into the interaction region. The efficiency for light collection is improved by a factor five as shown by comparing the present $n = 12$ measurements with $n = 7$ in I.

B. Microwave system and pressure measurement

In the single-oscillator measurements, rf power was fed into one X-band horn, and the other horn was terminated in a matched load. The X-band source used throughout the work was a Hewlett-Packard H01-694A sweep oscillator driving an Alfred 528A TWT amplifier. The sweeper was phase-locked to a Fluke 6160A frequency synthesizer for all but the $7\,^1D$-$7G$ measurements. During the latter, the sweeper was phase locked to a Micro-Now 101C frequency-multiplier chain (450 MHz output) based on a 5 MHz crystal. In addition, an OKI 24V11 600-mW klystron provided the second microwave frequency at 26 GHz and was phase locked to the synthesizer, as described in I. The X-band rf power was chopped and leveled by a Hewlett-Packard 8734B PIN modulator as in II.

In the $7\,^1D$-$7G$ measurements, only the X-band power was chopped, the 26-GHz rf power being left continuously on and the level adjusted manually as necessary. For the $16\,^1P$-$16\,^1D$ measurements reported in Sec. IV A the microwave system was identical to that described in II. rf power from the X-band and 26-GHz sources was measured with directional couplers and Hewlett-Packard X486A and K486A thermistor mounts and 431B power meters.

The helium pressure necessary to see a signal was provided by admitting ultrapure helium gas through a leak valve into the kinetic vacuum system, whose base pressure was 2×10^{-7} Torr. The helium pressure was monitored using the ion gauge during the measurements, but the gauge was calibrated for helium *in situ* using a CGS 1014A capacitance manometer. All helium pressures reported are absolute pressures, obtained by applying the calibration factor to the recorded ion-gauge readings.

The apparatus was otherwise as described in I as regards light collection, lock-in detection, signal averaging, etc.

IV. RESULTS: SINGLE-QUANTUM RESONANCES

A. $16\,^1P_1$-$16\,^1D_2$ resonance

As a comparison of the new and old experimental modules, we remeasured the $16\,^1P_1$-$16\,^1D_2$ resonance reported in II many times under a wide variety of experimental conditions. Whereas in the earlier work the resonance linewidths could not be reduced much below 6 MHz owing to Stark shifts in the interaction region, the FWHM in the new measurements was as low as 1.5 MHz; typical values ranged from 2.0 to 2.5 MHz. We take this to indicate that stray electric fields have been reduced by at least one-half. An average of 34 separate line-center determinations is given in Table I with an uncertainty equal to the standard deviation (SD) about the mean. The new value lies 0.5 MHz higher than that quoted in II, and the one-SD error bars of the new and old measurements meet without overlapping. This suggests that the −1.34 MHz Stark correction applied to the $n=16$ measurement in II was an overestimate, perhaps by a factor 2, although the new and old measurements are consistent.

TABLE I. Resonance frequencies of single-quantum resonances in ^{4}He.

Transition	Frequency (MHz) [a]	Other results (MHz) [b]	
$10\,^1D_2$-$10\,^1F_3$	10 918.825 ± 0.026	10 743 [c]	(T)
		10 916.5 ± 1.0 [d]	(E)
		10 918.6 ± 0.6 [e]	(E)
$10\,^1D_2$-$10\,^3F_3$	10 866.448 ± 0.026	10 692 [c]	(T)
		10 865.2 ± 1.0 [d]	(E)
		10 866.1 ± 0.5 [e]	(E)
$11\,^1D_2$-$11\,^1F_3$	8215.072 ± 0.082	8081 [c]	(T)
		8213.0 ± 1.0 [d]	(E)
		8215.0 ± 0.6 [e]	(E)
$11\,^1D_2$-$11\,^3F_3$	8175.526 ± 0.108	8043 [c]	(T)
		8173.5 ± 1.0 [d]	(E)
		8175.3 ± 0.5 [e]	(E)
$12\,^3D_1$-$12\,^3F_2$	9173.58 ± 0.18	9052.45 [c]	(T)
$12\,^3D_2$-$12\,^3F_3$	9179.76 ± 0.56	9058.15 [c]	(T)
$12\,^3D_3$-$12\,^3F_4$	9185.83 ± 0.21	9064.58 [c]	(T)
$12\,^3D_2$-$12\,^3F_2$	9193.72 ± 0.40	9073.02 [c]	(T)
$12\,^3D_2$-$12\,^1F_3$	9209.93 ± 0.34	9087.83 [c]	(T)
$6\,^1F_3$- $6\,^1G_4$	8854.06 ± 0.27	10 200 [f]	(E)
$16\,^1P_1$-$16\,^1D_2$	22 808.0 ± 0.2	22 807.5 ± 0.3 [g]	(E)

[a] Present work. Uncertainties are one standard deviation.
[b] E, experimental; T, theoretical.
[c] Chang and Poe, Refs. 13 and 14.
[d] Wing, Lea, and Lamb, Ref. 4.
[e] Prediction from fitting formula coefficients, MacAdam and Wing, Ref. 6.
[f] Optical data, Ref. 38.
[g] MacAdam and Wing, Ref. 6.

B. $n = 10$ and 11 ^1D-F resonances

Although the $10\,^1D_2$-$10\,^{1,3}F_3$ and $11\,^1D_2$-$11\,^{1,3}F_3$ resonances had been measured and reported previously by Wing, Lea, and Lamb,[4] the uncertainties (1.0 MHz) were larger than those routinely obtained in measurements[5,6] at $n = 6$, 7, and 8. Moreover, the $n = 10$ and 11 measurements appeared to lie systematically lower than expected on the basis of the $n = 6$–8 values, as illustrated in Figs. 2 and 3 of II. Therefore, we felt it desirable to improve the $n = 10$ and 11 measurements with the newly modified apparatus.

The results are listed in Tables I and II. The new $n = 10$ and 11 resonance centers lie 1–2 MHz higher than those reported by Wing, Lea, and Lamb,[4] which suggests that the earlier measurements were affected by Stark shifts caused by space charge or wall charging. The discrepancies of the earlier measurements amount to one-third or less of the FWHM in Ref. 4.

C. $12\,^3D$-$12F$ resonances

The $12\,^3D$-$12F$ resonance frequencies fell conveniently in the range of the X-band oscillator and offered an opportunity to resolve completely the fs of another ^3D and F state, the case $n = 7$ having already been reported in I. Our previous experience with such resonances ($n = 7$ in I and $n = 9$ in II) was borne out in that the $12\,^3D$-$12F$ resonances were quite weak in comparison with the $n\,^1D$-nF resonances in nearby n's. Resonances that correspond to all eight allowed transitions between the $12\,^3D$ and $12F$ fs levels were located. But owing to poor signal-to-noise ratios under even the optimum experimental conditions, the resonances originating from the closely spaced $12\,^3D_2$ and $12\,^3D_3$ levels could not be resolved from one another. The heights of the resonances connecting $12\,^3D_2$ to a $12F$ level ($J = 2$ or 3) were several times larger than those of the corresponding resonances that connect $12\,^3D_3$, a pattern seen previously in I and II. The $12\,^3D_2$-$12\,^3D_3$ splitting, based on a $1/n^3$ scaling of the $n = 7$ result,[5] is 1.40 ± 0.040 MHz, while the linewidths observed in the $12\,^3D$-$12F$ series ranged from 1.5 to 4 MHz. Consequently, in fitting the $12\,^3D_{2,3}$-$12\,^3F_3$, $12\,^3D_{2,3}$-$12\,^3F_2$, and $12\,^3D_{2,3}$-$12\,^1F_3$ resonance pairs, only one Lorentzian function was used and the result was attributed to the $12\,^3D_2$ level. In order to obtain the $12\,^3D$ fs values shown in Fig. 3, the $12\,^3D_2$-$12\,^3D_3$ splitting scaled from $n = 7$ was assumed. The mean resonance frequencies for the $12\,^3D$-$12F$ series are given in Table I. Derived fs intervals and comparisons with theoretical values are given in Table II. The complete fs scheme for the $12D$ and $12F$ states is shown in Fig. 2.

All quantitative measurements in the $12\,^3D$-$12F$ series were obtained at helium pressures low enough that the resonance polarity implied greater population in the $12\,^3D$ than in the $12F$ levels. We did verify, however, that the polarity reversal noted[5,6] for the $7\,^3D$-$7F$ and $9\,^3D$-$9F$ resonances at higher pressures takes place in $n = 12$ also.

D. $6F$-$6G$ resonances

The electric-dipole selection rules, together with the strong singlet-triplet mixing in helium states having $L \geq 3$ (F, G, etc.),[5,32] allow a total of eleven transitions between the four fs levels of the $6F$ state and the four fs levels of the $6G$ state, lying in the vicinity of 8.8 GHz. To detect the

TABLE II. Fine-structure intervals derived from measurements in Table I.

Interval	Frequency (MHz) [a]	Other results (MHz) [b]	
$10\,^1F_3$-$10\,^3F_3$	52.38 ± 0.04	50.78 [c]	(T)
		51.3 ± 1.4 [d]	(E)
		52.40 ± 0.13 [e]	(E)
$11\,^1F_3$-$11\,^3F_3$	39.55 ± 0.03	38.34 [c]	(T)
		39.5 ± 1.4 [d]	(E)
		39.70 ± 0.13 [e]	(E)
$12\,^3D_2$-$12\,^3D_1$	20.14 ± 0.44	20.57 [f]	(T)
$12\,^3F_3$-$12\,^3F_4$	4.68 ± 0.60	5.30 [f]	(T)
$12\,^3F_3$-$12\,^3F_2$	13.97 ± 0.69	14.87 [f]	(T)
$12\,^1F_3$-$12\,^3F_3$	30.17 ± 0.65	29.68 [f]	(T)

[a] Present work. Uncertainties are one standard deviation.
[b] T, theoretical; E, experimental.
[c] Chang and Poe, Ref. 13.
[d] Wing, Lea, and Lamb, Ref. 4.
[e] Prediction from fitting-formula coefficients, MacAdam and Wing, Ref. 6.
[f] Chang and Poe, Ref. 14.

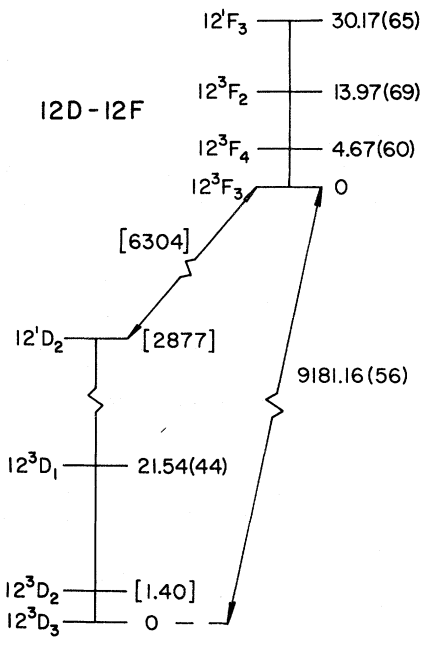

FIG. 2. Fine structure of ^{4}He 12D and 12F states (MHz). The numbers in square brackets are intervals not directly measured but deduced by scaling laws from our measurements in other n's. Results of the present work are shown with one-standard-deviation uncertainty in the last digit.

resonances it is necessary either to observe the ir fluorescence of the 6F or 6G states directly or, as we chose, to use a cascade such as $6F \rightarrow 5\,^1D \rightarrow 2\,^1P$ that retains selectivity between the 6F and 6G states while providing a shorter (visible) fluorescence wavelength. We therefore searched for and found one of the eleven resonances by monitoring the intensity of $5\,^1D$-$2\,^1P$ fluorescence at 4388 Å. Based on a scaling of the $n=7$, 9, and 10 D-G results discussed in Sec. V, it became perfectly clear that the $n=6$ resonance seen was $6\,^1F_3$-$6\,^1G_4$, others of the eleven lying at least 30 MHz above or below the observed resonance frequency. The resonance was very weak, as might be expected from the low efficiency of the cascade process used for detection and the small cross sections for electron-bombardment excitation. The polarity of the resonance indicated greater population in the $6\,^1F_3$ than in the $6\,^1G_4$ level at approximately 2×10^{-3} Torr. Higher pressure rendered the resonance unobservable, perhaps by a collision-induced equilibration of the 6F and 6G populations[33]; the signal also became unobservably small at lower pressures. None of the other ten allowed 6F-6G resonances could be located. The line center and uncertainty of the $6\,^1F_3$-$6\,^1G_4$ resonance are given in Table I. The linewidth was 4.5 MHz at an incident power 20 μW.

V. RESULTS: TWO-QUANTUM RESONANCES

A. $n=7,9$ ^1D-G resonances

A rough measurement of a $7\,^1D$-7G resonance was reported by Wing, Lea, and Lamb.[4] They saw the resonance by a second-order process in which electric fields generated by thermal motion of the atoms through a magnetic field of a few hundred gauss mixed the states of adjacent L values. In the zero magnetic field of the present experiments D-G transitions could be excited only by the two-quantum process whose theory is outlined in Sec. II. The frequency range thus indicated was scanned with the OKI 24V11 klystron at 26 GHz and the X-band sweep oscillator. Fluorescence from the $7\,^1D$ state at 4009 Å was monitored. The two resonances expected, $7\,^1D_2$-$7\,^1G_4$ and $7\,^1D_2$-$7\,^3G_4$, were easily located (signal-to-noise ratios 10 to 100) although they lay above the previous measurement and somewhat outside the reported error bar. The resonances were studied at various levels of saturation with 100–450 mW at 26 GHz and 3–90 mW at 11 GHz. The linewidths ranged from 2 to 4 MHz and the resonances displayed linear rf Stark shifts. The Stark-shift coefficients in terms of forward power in the waveguide were -4.0 ± 0.6 and $+3.4\pm0.2$ MHz/W for the 11 and 26 GHz perturbations, respectively. The line centers obtained after extrapolation to zero rf power are listed in Table III. The $7\,^1G_4$-$7\,^3G_4$ interval in Table IV is obtained by subtraction of the two $7\,^1D$-7G resonance frequencies with their SD's combined in quadrature.

Using a single oscillator at 8.8 GHz, we easily located the two-quantum resonances $9\,^1D_2$-$9\,^1G_4$ and $9\,^1D_2$-$9\,^3G_4$ at frequencies near the values predicted by a $1/n^3$ scaling of the $n=7$ results. The fluorescence of the $9\,^1D$ state was monitored at 3872 Å. A tracing of the two resonances obtained using a chart recorder is shown in Fig. 3. The rf power was varied from 5 to 60 mW, and the line centers shifted accordingly with a slope 30.8 ± 0.7 MHz/W. The extrapolated resonance centers are listed in Table III. The $9\,^1G_4$-$9\,^3G_4$ interval listed in Table IV was obtained by subtraction of the zero-power $9\,^1D$-9G resonance frequencies.

B. $10\,^3D$-10G resonances

Only two transitions in $n\,^1D$-nG are allowed by the electric-dipole selection rules for each n; one of these, $n\,^1D_2$-$n\,^3G_4$, is further allowed only by virtue of the strong singlet-triplet mixing in helium G states having $J=L$. Therefore, neither the $n=7$ nor $n=9$ measurements just described would allow the complete determination of fs in an nG

TABLE III. Resonance frequencies of two-quantum resonances in ^{4}He. Measured line centers have been extrapolated to zero rf power.

Transition	Frequency (MHz) [a]	Other results (MHz) [b]
$7\,^1D_2$-$7\,^1G_4$	37 261.012 ± 0.033	37 090 ± 70 [c] (E)
$7\,^1D_2$-$7\,^3G_4$	37 184.724 ± 0.047	37 090 ± 70 [c] (E)
$9\,^1D_2$-$9\,^1G_4$	17 697.065 ± 0.041	
$9\,^1D_2$-$9\,^3G_4$	17 661.096 ± 0.022	
$10\,^3D_1$-$10\,^3G_3$	17 798.57 ± 0.29	
$10\,^3D_2$-$10\,^3G_4$	17 814.30 ± 0.43	
$10\,^3D_3$-$10\,^3G_4$	17 816.58 ± 0.67	
$10\,^3D_3$-$10\,^3G_5$	17 826.97 ± 0.11	
$10\,^3D_2$-$10\,^3G_3$	17 833.89 ± 0.31	
$10\,^3D_2$-$10\,^1G_4$	17 840.15 ± 0.25	
$10\,^3D_3$-$10\,^1G_4$	17 842.42 ± 0.27	

[a] Present work. Uncertainties are one standard deviation.
[b] E, experimental.
[c] Wing and Lamb, Ref. 3. The $7F$-$7G$ interval reported is taken to be the interval between the $7\,^{1,3}F_3$ mean and the $7\,^{1,3}G_4$ mean.

state. There have been no previous measurements of G-state fs. However, measurements of $n\,^3D$ and nF fs[5,6] have indicated that the Breit-Bethe theory[5] of relativistic fs can provide a useful first approximation, a fact that aided us in the identification of the $10\,^3D$-$10G$ resonances.

Seven of the eight allowed $10\,^3D$-$10G$ two-quantum resonances near 17.8 GHz were found; $10\,^3D_3$-$10\,^3G_3$ was obscured by noise. A single oscillator at 8.9 GHz was used, and the fluorescence of the $10\,^3D$ state was monitored at 3554 Å. The resonances, like the previous $n\,^3D$ resonances measured, were weak. However, all fs splittings in the $10\,^3D$ and $10G$ states were determined, including the small $10\,^3D_2$-$10\,^3D_3$ interval. The rf power was varied from 6.5 to 25 mW; the linewidths ranged from 1.5 to 4.5 MHz. The signal-to-noise ratios varied from 5 to 15.

The results after extrapolation to zero rf power are listed in Table III. The fs intervals are listed in Table IV and illustrated in Fig. 4.

C. $16\,^1P$-$16F$ resonances

The two-quantum resonances $16\,^1P_1$-$16\,^1F_3$ and $16\,^1P_1$-$16\,^3F_3$ were sought and found by use of a single oscillator at 10.0 GHz. The data were of poor quality, probably because of the severe dc Stark shifts experienced by the $16F$ states. [An unobservable hypothetical 10-kHz Stark shift in

TABLE IV. Fine-structure intervals derived from two-quantum resonances, Table III.

Interval	Frequency (MHz) [a]	Other results (MHz) [b]
$7\,^1G_4$-$7\,^3G_4$	76.29 ± 0.06	76.21 [c] (T)
		76.19 [d] (T)
$9\,^1G_4$-$9\,^3G_4$	35.97 ± 0.05	35.86 [c] (T)
		35.85 [d] (T)
$10\,^3D_3$-$10\,^3D_2$	2.28 ± 0.30	1.94 [e] (T)
$10\,^3D_3$-$10\,^3D_1$	37.59 ± 0.52	37.50 [e] (T)
$10\,^3G_4$-$10\,^3G_5$	10.39 ± 0.68	10.38 [c] (T)
$10\,^3G_4$-$10\,^3G_3$	19.58 ± 0.53	19.82 [c] (T)
$10\,^1G_4$-$10\,^3G_4$	25.84 ± 0.51	26.14 [c] (T)
		26.31 [d] (T)
$16\,^1F_3$-$16\,^3F_3$	12.4 ± 0.6	13.19 ± 0.07 [f] (E)

[a] Present work. Uncertainties are one standard deviation.
[b] E, experimental; T, theoretical.
[c] Breit-Bethe theory outlined in MacAdam and Wing, Ref. 5.
[d] Chang and Poe, Ref. 13.
[e] Chang and Poe, Ref. 14.
[f] Prediction from fitting-formula coefficients, MacAdam and Wing, Ref. 6.

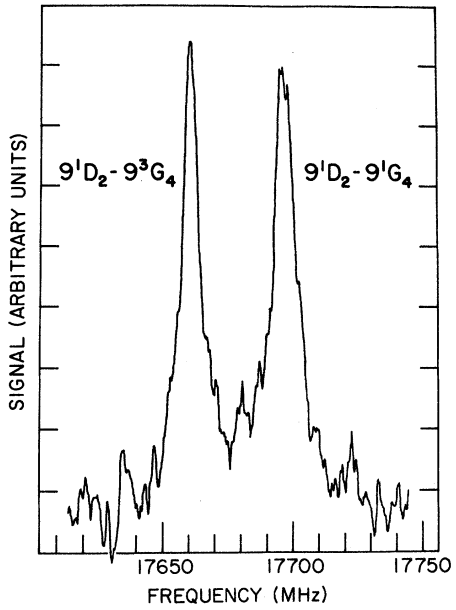

FIG. 3. Chart recorder trace of the $9\,^1D_2$-$9\,^{1,3}G_4$ resonances. The resonances are power-broadened by a factor 2 to 3 for purposes of display. Sweep rate 0.4 MHz/sec, lock-in time constant 2 sec.

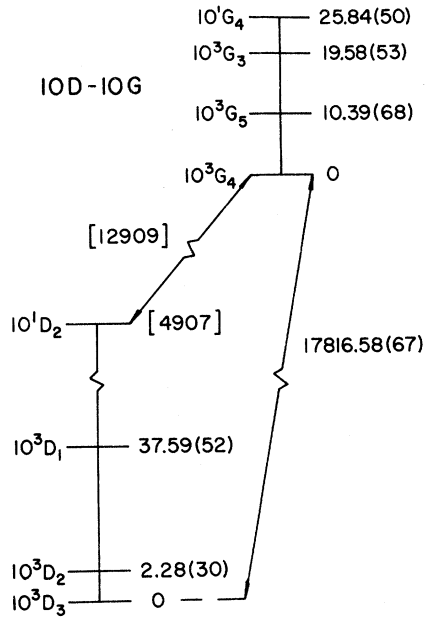

FIG. 4. Fine structure of ^{4}He $10D$ and $10G$ states (MHz). Notation as in Fig. 4.

the $10F$ state at 40 eV bombarding energy would scale by n^7 and the square of bombarding voltage (either from wall charging or from space charge) so as to be greater than 1 MHz in $n=16$ at 80 eV.] The $16\,^1F_3$-$16\,^3F_3$ interval was obtained by subtracting the $16\,^1P_1$-$16\,^1F_3$ and $16\,^1P_1$-16^3F_3 resonance frequencies measured under identical experimental conditions; three such determinations showed a scatter of 1 MHz. Although the resonance frequencies themselves are not of useful accuracy, and are not included in Table III, the weighted average of the three determinations of the $16\,^1F_3$-$16\,^3F_3$ interval is listed in Table IV.

VI. DISCUSSION

A. Series formulas

In I and II we listed coefficients A, B, and C for fitting formulas

$$\nu_n = A/n^3 + B/n^5 + C/n^7 \qquad (3)$$

that represented best fits to the available data for resonances of given types, e.g., $n\,^1D_2$-$n\,^1F_3$. The new measurements reported in this paper allow the published coefficients to be revised and coefficients to be given for new resonance series.

The new $n=10$ and $n=11$ measurements result in fits of $n\,^1D_2$-$n\,^1F_3$ and $n\,^1D_2$-$n\,^3F_3$ series whose D's are reduced from approximately 1 MHz to 0.1 MHz. With the new results, $n=12$ can be added to the data set for the $n\,^1F_3$-$n\,^3F_3$ series, and the improved $n=10$ and 11 members can be substituted for the earlier data. The new parameters for these series are given in Table V.

Two series $n\,^3D_2$-$n\,^{1,3}F_3$ can be constructed from the $n=7$ and 9 results reported in I and II, respectively, and $n=12$ reported in this paper. The results are listed in Table V.

A series formula for $n\,^1F_3$-$n\,^1G_4$ intervals can be constructed from the new $n=6$, 7, 9, and 10 data. The $7\,^1D_2$-$7\,^1F_3$ result of Wing and Lamb[3] is subtracted from the $7\,^1D_2$-$7\,^1G_4$ result listed in Table III, which yields the $7\,^1F_3$-$7\,^1G_4$ interval. The predictions of the fitting formulas (Table V) are used to convert the present $n=9$ and 10 results (Table III) to the corresponding $n\,^1F_3$-$n\,^1G_4$ intervals; and the $n=6$ member of the series is included, as measured directly (Table I). The resulting coefficients are listed in Table V. Related series $n\,^3F_3$-$n\,^3G_4$ and $n\,^1G_4$-$n\,^3G_4$ are constructed from $n=7$, 9, and 10 data in the same way.

In II we showed how the variance-covariance matrix[34] that resulted from the least-squares fit of each resonance series could be used to estimate the uncertainties of predictions for series members not measured. Figure 5 shows such results in the form of prediction-error bands for the $n\,^1F_3$-$n\,^1G_4$ series. The error bands demonstrate that, on the basis of the present four measure-

TABLE V. Constants for the fitting formula Eq. (3).

Transition	Data used[a]	A (GHz)	B (GHz)	C (GHz)
$n\,^1D_2$-$n\,^1F_3$	$n=6$–8, 10, 11	11009.108	−9015.723	−1447.345
$n\,^1D_2$-$n\,^3F_3$	$n=6$–8, 10, 11	10954.118	−8727.208	−4010.181
$n\,^1F_3$-$n\,^3F_3$	$n=6$–12, 16	54.691	−256.020	1773.637
$n\,^1F_3$-$n\,^1G_4$	$n=6, 7, 9, 10$	2076.166	−5867.497	−909.489
$n\,^3F_3$-$n\,^3G_4$	$n=7, 9, 10$	2106.511	−6364.955	8182.989
$n\,^1G_4$-$n\,^3G_4$	$n=7, 9, 10$	22.198	527.217	−16303.314
$n\,^3D_2$-$n\,^1F_3$	$n=7, 9, 12$	16123.036	−29875.639	−16746.978
$n\,^3D_2$-$n\,^3F_3$	$n=7, 9, 12$	16071.171	−29975.049	−7996.311

[a] Data taken from I, II, and the present work.

ments, the entire series can be predicted reliably within about 75 ppm.

B. Electrostatic and relativistic fine structure

The most accurate calculations of electrostatic fs in helium Rydberg states are those of Chang and Poe.[13,14] Recently, they published their results for D- and F-state fs, in the form of coefficients for series formulas that have the form of Eq. (3).[14] By comparing the corresponding coefficients that describe the experimental and theoretical results, we can attribute the discrepancies to particular powers of n. In the $n\,^1D_2$-$n\,^1F_3$ series, the theoretical values of coefficients A and B in Eq. (3) are too small by 1.70% and 14.7% respectively. The theoretical value of coefficient C is 20 times the experimental value in Table V but represents only a small part of the total discrepancy between theory and experiment, because of the high exponent of n in the third term of Eq. (3). A, B, and C calculated by Chang and Poe for the $n\,^3D_2$-$n\,^1F_3$ series differ from the experimental values by −1.34%, −3.13%, and +85% respectively.

Deutsch[35] has recently used a polarization theory to calculate the nonrelativistic (i.e., spin-independent) displacements of $(1snl)nL$ levels in helium from the Bohr levels for $l \geq 2$ and $3 \leq n \leq 9$. For comparison of his nF-nG intervals with experiment, we must calculate the averages of F- and G-state fs patterns, using the level degeneracies as weighting factors. The results, shown in Table VI, demonstrate that the polarization-theory results are in moderately good agreement with experiment but, like the calculated values of Chang and Poe, are systematically too small. Deutsch's results scale exactly as $A/n^3+B/n^5$, thus allowing a direct comparison of coefficients A and B between theory and experiment.[36] The polarization-theory values of A and B are smaller than the experimental values implied by the data in Table VI by 5.7% and 25%, respectively.

The Breit-Bethe theory[37] of helium relativistic fs was described in I. It was shown there that, although not of high accuracy for low l, the theory provides a useful starting point that agrees moderately well with experiment. Recently, Derouard *et al.*[12] have measured the off-diagonal matrix element of the spin-orbit interaction (see I, Table I) connecting $n\,^1D$ and $n\,^3D$ states ($n=3$–8) and have shown that the Breit-Bethe values are correct within the experimental uncertainty (about 8%). In I, we showed that the Breit-Bethe fs predictions in the 7 ^3D term were approximately correct regarding the balance between spin-orbit and spin-spin contributions but that the over-all scale of the fs was about 5% too large. In the 7F state, the predictions were 19% too large. The $n\,^1D_2$-$n\,^3D_2$ and $n\,^1F_3$-$n\,^3F_3$ intervals depend in a major way on exchange integrals and therefore could not be cal-

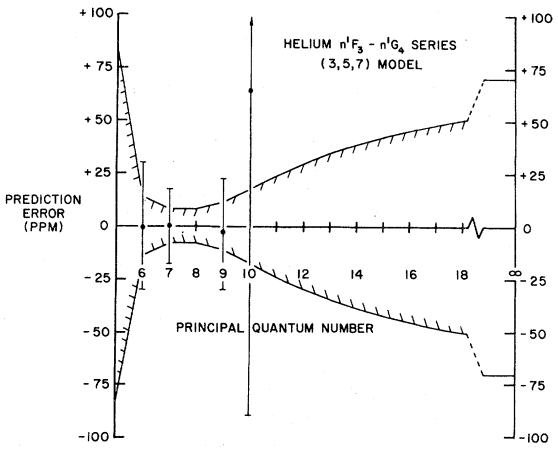

FIG. 5. Error bands for predictions of $n\,^1F_3$-$n\,^1G_4$ intervals in ^{4}He. The hatched lines represent the one-standard-deviation uncertainties for predictions based on the coefficients in Table V, using the (3, 5, 7) model, i.e., Eq. (3). The data points represent the discrepancies between our measurements and the predicted frequencies.

TABLE VI. Comparison of measured nF-nG intervals with polarization-theory results. The experimental nF-nG intervals are obtained by combining transition frequencies measured in the present work with our previous results, Refs. 5 and 6. Where nF or nG fs was not measured directly, the fs averages are based on $1/n^3$ scaling from measured fs.

	Experimental (MHz) [a]	Theory (MHz) [b]	Theory/Expt.
$6F_{av}-6G_{av}$	8831.7±0.3	8450	0.957
$7F_{av}-7G_{av}$	5686.5±0.2	5430	0.955
$9F_{av}-9G_{av}$	2741.1±0.3	2610	0.952
$10F_{av}-10G_{av}$	2013.6±0.6	1920	0.954

[a] The experimental values include corrections that compensate for direct and exchange Coulomb interactions, estimated from Ref. 13, and the (hydrogenic) relativistic variation of mass with velocity (Ref. 37). The corrected intervals should then be directly comparable with polarization theory.

[b] Deutsch, Ref. 35.

culated from the Breit-Bethe theory alone.

Because the nonrelativistic singlet-triplet G difference (exchange-like contributions only) is negligible, owing to the non-overlap of ng and $1s$ orbitals,[13] our $10G$ data offer a new opportunity for comparison of the Breit-Bethe theory with experiment, encompassing both $10\,^1G$ and $10\,^3G$ terms. We find that the Breit-Bethe predictions in the $10G$ state are correct within the experimental uncertainty. Excellent agreement of the singlet-triplet intervals is also obtained in $7G$ and $9G$ between the experimental results and both the Breit-Bethe theory and the calculations of Chang and Poe.[13] The experimental and theoretical results are compared in Table IV.

From the series-formula coefficients in Chang and Poe's recent D and F state fs calculations,[14] we have calculated the $10\,^3D$, $12\,^3D$, and $12\,^3F$ fs intervals for comparison with experiment in Tables II and IV.

ACKNOWLEDGMENT

We would like to thank Nasrat Raouf for help in data taking.

†Work supported in part by the National Science Foundation and by a contract from the Al Hazen Research Institute, Baghdad, Iraq, for joint research with the University of Arizona.

[1]W. H. Wing, D. L. Mader, and W. E. Lamb, Jr., Bull. Am. Phys. Soc. 16, 531 (1971).

[2]W. E. Lamb, Jr., D. L. Mader, and W. H. Wing, in *Fundamental and Applied Laser Physics, Proceedings of the Esfahan Symposium*, edited by M. S. Feld, A. Javan, and N. A. Kurnit (Wiley, New York, 1973), pp. 523–538.

[3]W. H. Wing and W. E. Lamb, Jr., Phys. Rev. Lett. 28, 265 (1972).

[4]W. H. Wing, K. R. Lea, and W. E. Lamb, Jr., in *Atomic Physics 3*, edited by S. J. Smith and G. K. Walters (Plenum, New York, 1973), pp. 119–141.

[5]K. B. MacAdam and W. H. Wing, Phys. Rev. A 12, 1464 (1975), referred to in the text as I.

[6]K. B. MacAdam and W. H. Wing, Phys. Rev. A 13, 2163 (1976), referred to in the text as II.

[7]W. E. Lamb, Jr., and T. M. Sanders, Phys. Rev. 119, 1901 (1960).

[8]L. R. Wilcox and W. E. Lamb, Jr., Phys. Rev. 119, 1915 (1960).

[9]J. P. Descoubes, in *Physics of the One and Two Electron Atoms*, edited by F. Bopp and H. Kleinpoppen (North-Holland, Amsterdam, 1969), p. 341.

[10]H. G. Berry, J. L. Subtil, and M. Carre, J. Phys. (Paris) 33, 947 (1972); H. G. Berry and J. Subtil, Nucl. Instrum. Methods 110, 321 (1973).

[11]T. A. Miller, R. S. Freund, F. Tsai, T. J. Cook, and B. R. Zegarski, Phys. Rev. A 9, 2974 (1974); T. A. Miller, R. S. Freund, and B. R. Zegarski, *ibid.* 11, 753 (1975).

[12]J. Derouard, R. Jost, M. Lombardi, T. A. Miller, and R. S. Freund, Phys. Rev. A 14, 1025 (1976).

[13]T. N. Chang and R. T. Poe, Phys. Rev. A 10, 1981 (1974).

[14]T. N. Chang and R. T. Poe, Phys. Rev. A 14, 11 (1976).

[15]H. J. Beyer and K. J. Kollath, J. Phys. B 8, L326 (1975); 9, L185 (1976).

[16]H. J. Beyer and K. J. Kollath (private communication).

[17]"Search and Discovery," Physics Today 28 (No. 11), 17 (1975).

[18]S. Haroche, M. Gross, and M. P. Silverman, Phys. Rev. Lett. 33, 1063 (1974); C. Fabre, M. Gross, and S. Haroche, Opt. Commun. 13, 393 (1975).

[19]T. F. Gallagher, R. M. Hill, and S. A. Edelstein, Phys. Rev. A 13, 1448 (1976).

[20]K. Fredriksson and S. Svanberg, J. Phys. B 9, 1237 (1976).

[21]C. D. Harper and M. D. Levenson, Phys. Lett. 56A, 361 (1976).

[22]Y. Kato and B. P. Stoicheff, J. Opt. Soc. Am. 66, 490

(1976); B. P. Stoicheff and Y. Kato, J. Opt. Soc. Am. 65, 1180 (1975).
[23]T. F. Gallagher, R. M. Hill, and S. A. Edelstein, Phys. Rev. A 14, 744 (1976).
[24]A. F. J. van Raan, G. Baum, and W. Raith, J. Phys. B 9, L173 (1976).
[25]M. G. Littman, M. L. Zimmerman, T. W. Ducas, R. R. Freeman, and D. Kleppner, Phys. Rev. Lett. 36, 788 (1976).
[26]H. Salwen, Phys. Rev. 99, 1274 (1955).
[27]J. Brossel, J. Margerie, and J. Winter, C. R. Acad. Sci. (Paris) 241, 556 (1955); and J. Winter, *ibid.* 241, 600 (1955).
[28]N. F. Ramsey, Phys. Rev. 100, 1191 (1955).
[29]D. T. F. Marple and J. W. Trishka, Phys. Rev. 103, 597 (1956).
[30]J. H. Shirley, Phys. Rev. 138, B979 (1965).
[31]The cathodes were obtained from Philips Elmet Corp., Lewiston, Maine, part number PE-2.
[32]R. K. van den Eynde, G. Wiebes, and T. Niemeyer, Physica (Utr.) 59, 401 (1972).
[33]T. F. Gallagher, S. A. Edelstein, and R. M. Hill, Phys. Rev. Lett. 35, 644 (1975).
[34]W. C. Hamilton, *Statistics in Physical Science* (Ronald, New York, 1964).
[35]C. Deutsch, Phys. Rev. A 13, 2311 (1976).
[36]In Ref. 35, factors $l+1$ and $\overline{l}$ were omitted from the denominators of Eqs. (3) and (4) respectively, as can be verified by comparison with K. Bockasten, Phys. Rev. A 9, 1087 (1974). The numerical results in Tables I and II of Ref. 35 were, however, calculated using the correct formulas.
[37]H. Bethe and E. Salpeter, *Quantum Mechanics of One- and Two-Electron Atoms* (Springer, Berlin, 1957).
[38]W. C. Martin, J. Phys. Chem. Ref. Data 2, 257 (1973).